

Boltzmann equation description of flows at long mean free paths

J. Feng* and W. N. G. Hitchon

Department of Electrical and Computer Engineering, University of Wisconsin–Madison, Madison, Wisconsin 53703, USA

(Received 7 September 2003; published 24 September 2004)

The flow of a gas around a rectangular object is simulated by solving the Boltzmann equation for the gas. The Boltzmann equation is solved by means of a method of characteristics which we refer to as a convective scheme (CS). This paper focuses, first, on two computational issues. We describe how the CS which is presented here is implemented so as to handle reflecting boundary conditions very accurately. Next, a collision operator for the self-collisions of the neutral gas has been developed which conserves momentum and energy “exactly” and which also preserves higher moments of the distribution so as to correctly calculate quantities such as viscosity. Finally, the method is illustrated briefly by calculating flow patterns and drag coefficients for a low Mach-number flow around a rectangular obstacle, over a range of Knudsen numbers which spans the transitional regime, and very accurate values of the drag coefficient are obtained across the whole range.

DOI: 10.1103/PhysRevE.70.036704

PACS number(s): 02.70.-c, 47.11.+j, 47.45.-n

I. INTRODUCTION

A variety of devices which operate at atmospheric pressure, but which are microscopic in dimension (having dimensions of order microns) involve gas flows where the dimensions of the device (denoted by L) are comparable to the mean free path of the gas λ [1–3]; the Knudsen number $K_n = \lambda/L$ is of order unity. In this work we shall examine flows where K_n ranges from about 0.05 to about 10. Examples of such devices include microscopic pumps which are envisaged in future, and microscopic aircraft—although full-size aircraft which operate at very high altitude might also fall into this category.

The conventional techniques for describing these flows are what are referred to as “particle” simulations. In this paper we consider an alternative, which is to develop a sufficiently accurate direct method of solution of the Boltzmann equation (BE)

$$\frac{\partial f}{\partial t} + \mathbf{v} \cdot \frac{\partial f}{\partial \mathbf{r}} + \mathbf{a} \cdot \frac{\partial f}{\partial \mathbf{v}} = \left(\frac{\partial f}{\partial t} \right)_c, \quad (1)$$

where f is the particle distribution function $f(\mathbf{r}, \mathbf{v}, t)$, t is the time, \mathbf{r} and \mathbf{v} are the coordinates for the state space, \mathbf{a} is the acceleration vector field, and $(\partial f / \partial t)_c$ is the collision operator [4]. Particle methods such as direct simulation Monte Carlo (DSMC) and the information preserving (IP) [5,6] form of DSMC have somewhat different strengths and weaknesses as opposed to the solution of the BE. Broadly speaking, particle methods suffer from statistical noise, whereas a solution of the BE will usually have some amount of inaccuracy due to numerical diffusion. The method we present here, which is a version of the method of characteristics which we call a “convective scheme” (CS), minimizes numerical diffusion in a variety of ways [7–9] but cannot eliminate it entirely. The CS was originally developed for use in plasma simulation. A brief introduction to the CS is pre-

sented in the appendices. The above remarks about particle methods and solution of the BE apply in that context also. A particle method does well in describing a narrow beam, since it resolves the position of the particles in the beam better than a mesh based solution of the BE. On the other hand, the tail of a distribution of particles may contain a very small fraction of the particles but those particles may be critically important (for instance, they may cause all the ionization.) In such a situation, the particle method may not be able to resolve the tail as well as solving the BE does. Similarly, even the very efficient IP method has some difficulty in avoiding statistical fluctuations in density when it is applied to low Mach number flows at values of K_n of order unity. The purpose of this work, then, is to discuss an alternative to particle methods, which may be useful in some circumstances where they are less effective. In other situations particle methods will be preferred.

The BE can be solved by finite difference approaches, in what is typically an Eulerian scheme [10,11]. Finite differences (FDs) are less accurate than a method of characteristics, such as that employed here, because they are limited by the Courant criteria to rather small time steps. The use of small time steps not only makes calculations slow, but it leads to significant numerical diffusion. (In a steady state calculation similar difficulties arise for essentially the same reasons.) In addition, FDs necessarily involve calculating derivatives of the distribution, something that is best avoided since the gradients can be very large indeed, and again lead to inaccuracy in a FD approach.

The CS described here is a method of characteristics, and the principal difficulty associated with it is the handling of boundary conditions, since the correct form of the propagator is not always clear at a boundary. A method of images can be used—but again, this is difficult to set up at a complex boundary. In what follows we show how simple boundaries may be handled very accurately. Complex boundaries have been implemented in the CS previously, for an unstructured (triangular) mesh [12,13]. The methods used here extend naturally to complex boundaries made up of small rectangular cells.

*Author to whom correspondence should be addressed.

Email address: fengj@circe.engr.wisc.edu

The collision operator used here assumes that the distribution is relaxing to a Maxwellian, with the temperature of the Maxwellian being determined to conserve the energy of the scattered particles, according to a Krook (or Bhatnagar-Gross-Krook) collision term. The essential point is not the exact form of the collision operator, however. Any form for the collision integrals could be employed. The issue which causes difficulty, and which we address here, is that of how to ensure that all appropriate conservation laws may be satisfied to numerical accuracy, for an arbitrary form of the collision integral. To this end, we have chosen to allow the distribution to be relaxing to a drifting Maxwellian, but the procedure is equally applicable, whatever the form of the collision operator.

The CS was designed to minimize numerical diffusion by exploiting the long time steps available to a method of characteristics and by a variety of other methods. It focuses on each initial cell on the mesh, and maps that cell back after one or multiple time step(s) in such a way as to conserve particles, momentum and energy exactly and locally in phase space. Usually the particles are considered to move in a packet from their initial cell for a time step which is small compared to a collision time, during which a fraction of them suffer collisions and after which they all are mapped back to the phase space mesh. A version of the CS where the phase space is redundantly covered with a set of long-lived moving cells has been used to reduce numerical diffusion even further. The point of this work was to allow the particles to travel in their packets along the characteristics for many mean free paths. Allowing the packets to persist for multiple time steps reduces numerical diffusion but it means that multiple packets cover any point in phase space.

These issues have been discussed at length previously [9,14]. In this work our focus in implementing the method was twofold: (1) to handle reflecting boundaries extremely accurately, in a sense which will be defined below, and (2) to implement a collision operator which preserves the critical features of the flow—again, to very high accuracy. These topics are the subjects of Secs. II and III. Section IV will briefly present results for the flow fields and drag coefficients for a test case, which consists of flow around a rectangular obstacle. Conclusions are given in Sec. V.

II. KINETIC MODEL OF THE SYSTEM

The system under study is a neutral gas flow in the xy plane with translational symmetry in z . To properly treat collisions three independent parameters are used in describing the particles' velocity. The model is of two dimensions in space and three dimensions in velocity. The effect of gravity is neglected, so the acceleration term \mathbf{a} in the BE (1) will be zero. In this section we first discuss the structure of the mesh, followed by a description of the handling of reflections off surfaces in the method of characteristics and the remapping rules.

A. Mesh structure for the convective scheme and the ballistic motion

For each time step Δt , each cell will move “ballistically” (i.e., collisionlessly) first, then a fraction $\nu\Delta t \ll 1$ of the par-

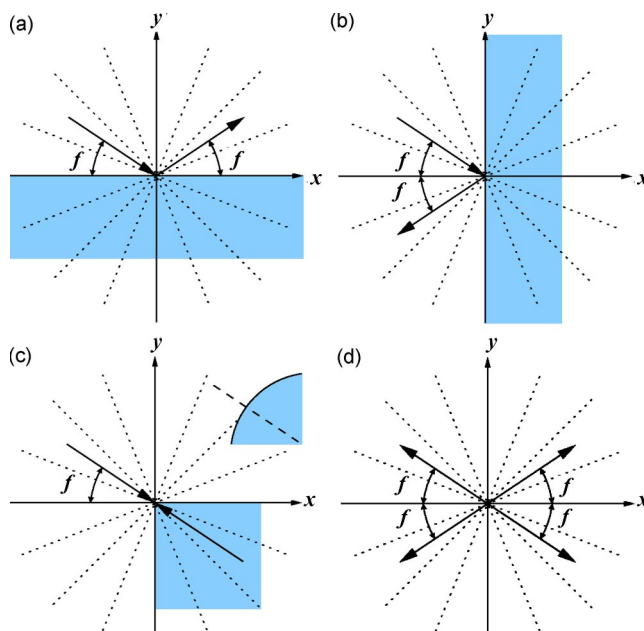


FIG. 1. Specular reflections and the mesh structure. When a moving cell hits an obstacle, the direction of reflection follows Snell’s reflection law. Corners are treated as infinitesimal spheres, so the reflection direction will be opposite to the incident direction. Incident and reflection directions are thus arranged to coincide with grid points in the velocity mesh to reduce numerical error.

ticles in the cell will be scattered [7–9]. The handling of the scattered particles will be discussed in the next section.

The design of the mesh is in general intended to minimize the numerical diffusion when moving the cells ballistically and/or during collisions. We choose (v, μ, ϕ) as the coordinate system for the velocity space, where v is the speed, μ is the cosine of the angle between the velocity and the positive z axis, and ϕ is the azimuthal angle of the velocity projection on the xy plane. If a cell does not hit a boundary, then its velocity does not change, since there is no external force field. When it is re-mapped back to the mesh after ballistic motion, the numerical diffusion will only involve spatial cells; there is no numerical diffusion over velocity. Hence our velocity space variables can be chosen to minimize numerical diffusion during collisions. This is accomplished by using (v, μ, ϕ) as discussed in Ref. [15].

The obstacle to the flow is composed of horizontal and vertical planes. A cell coming in at the angle $2\pi - \phi$ (or $-\phi$) will bounce back in the ϕ direction if there is a horizontal plane in the path, as shown in Fig. 1(a). The case of a vertical plane is shown in Fig. 1(b). Care must be taken for cells which reflect at corner points. The incident plane is ill defined at corners; we assume the corner is a round surface, as shown in Fig. 1(c), such that the incoming cell will rebound in the opposite direction. Corners are singular points, in mathematical terms they are a (Lebesgue) measure zero set, so reflections off corners will be extremely rare. As a result of the method used for reflection, if ϕ corresponds to a grid point on the mesh, so do $-\phi$, $\pi - \phi$, and $\pi + \phi$ shown in Fig. 1(d).

Fairly complex geometry objects can be constructed using horizontal, vertical, and 45° oblique planes in two-

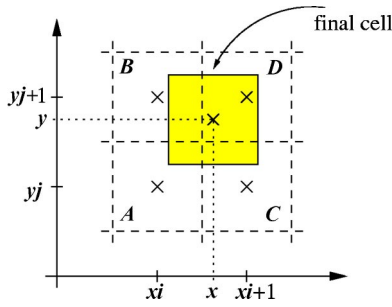


FIG. 2. Re-mapping of a final cell to mesh cells A, B, C, D . The fraction of particles mapped to a mesh cell is proportional to the overlapping area between the final cell and the mesh cell. Without an external force field, the velocity of the particles is constant, so the velocity indices of the mesh cells are the same as those of the final cell.

dimensional cases. To generalize the previous observation, if there are planes in the domain that are at 45° to the main axes, we can arrange the grid points of the azimuthal angle so as to match the rebound angles. As a result, ballistic motion will not produce any numerical diffusion in the velocity space.

B. Reflection and re-mapping rules

Once the mesh structure is defined, rules to map back the unscattered particles in the final cell back to each mesh cell can be constructed. This has been discussed at length previously [9]. If the final cell does not overlap any forbidden cells, the fraction of the particles that is mapped back to each mesh cell is proportional to the overlapped area. As shown in Fig. 2, the final cell at (x, y) has N particles with velocity $(v|_k, \mu|_\ell, \phi|_m)$. We will map the particles to the mesh cells (A, B, C , and D) shown, with the same velocity $(v|_k, \mu|_\ell, \phi|_m)$, according to the following rules:

$$N_A = N \left(1 - \frac{x - x_i}{\Delta x} \right) \left(1 - \frac{y - y_j}{\Delta y} \right), \quad (2)$$

$$N_B = N \left(1 - \frac{x - x_i}{\Delta x} \right) \left(\frac{y - y_j}{\Delta y} \right), \quad (3)$$

$$N_C = N \left(\frac{x - x_i}{\Delta x} \right) \left(1 - \frac{y - y_j}{\Delta y} \right), \quad (4)$$

$$N_D = N \left(\frac{x - x_i}{\Delta x} \right) \left(\frac{y - y_j}{\Delta y} \right), \quad (5)$$

where Δx and Δy are the cell sizes in the x and y directions, respectively.

The CS describes particles which travel in groups, which we refer to as “moving cells” (MCs). The MCs originate in single cells of the mesh, with a particular range in space (i.e., shape) and discrete velocities; and they are launched at discrete times. On reflection, particles are moved from one MC into another. The reflected particles behave as if they came from cells of the mesh, although some of the source cells

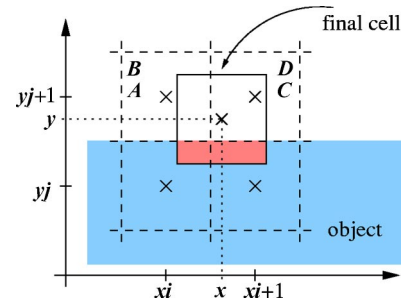


FIG. 3. Re-mapping of a final cell to mesh cells at a horizontal boundary. The heavily shaded area marks the part of the final cell overlapping the obstacle. Cells A and C are reflected cells, which went into the shaded area. The position of the final cell which went into the shaded area determines the fraction of the particles which is reflected, according to Eqs. (2)–(5). Mesh cells A and B have the same index in configuration space, but the velocity of cell A is mirrored vertically. The same situation applies to mesh cells C and D .

will be “virtual” cells which lie behind the reflecting surface. The flux produced by the reflection, which acts as if it comes from the virtual cells, should produce a flux such that a homogeneous isotropic gas above the surface is still homogeneous and isotropic after reflection. To do this the virtual cells (if they are explicitly constructed) must simply extend the real mesh behind the surface without any discontinuities. Other strategies are possible, but this is a relatively simple one.

In specular reflection, when the final cell, with velocity $(v|_k, \mu|_\ell, \phi|_m)$, overlaps horizontal boundary mesh cells as shown in Fig. 3, Eqs. (2)–(5) still apply. The portion of the final cell which overlapped the shaded area is placed in the shaded area, according to Eqs. (2)–(5), but is then reflected into cells A and C . Mesh cells A and B have the same indices as each other on the configuration space mesh $(x|_i, y|_{j+1})$ with different indices on the velocity space mesh: $(v|_k, \mu|_\ell, \phi|_m)$ for B and its mirror velocity $(v|_k, \mu|_\ell, \pi - \phi|_m)$ for A . Likewise, mesh cells C and D have the same indices as each other on the configuration space mesh, $(x|_{i+1}, y|_{j+1})$, with different indices on the velocity space mesh. Similar rules can be constructed for the vertical boundary case. If the final cell, with velocity $(v|_k, \mu|_\ell, \phi|_m)$, overlaps a corner mesh cell as shown in Fig. 4, Eqs. (2)–(5) still apply, where mesh cells B and C have the same indices as each other on the configuration space mesh $(x|_i, y|_{j+1})$ with different indices on the velocity space mesh: $(v|_k, \mu|_\ell, \phi|_m)$ for B and the *opposite* velocity $(v|_k, \mu|_\ell, \phi|_m + \pi)$ for C . Since cells which overlap a corner can come from all directions except for the direction from the obstacle, inverting the velocity of the particles in the part of MC which overlaps the obstacle is consistent with what we described before in Fig. 1(d). These rules for specular reflection mean that a uniform gas with no flow velocity remains in that state when it reflects off an obstacle.

To simulate viscous flow in the vicinity of the boundary, cells can reflect from the boundary *diffusely*. A *nonslip* condition is usually assumed in fluid mechanics. The counterpart in kinetic theory consists of diffuse reflection. In the fully diffuse reflection case, as shown in Fig. 5 for a horizontal

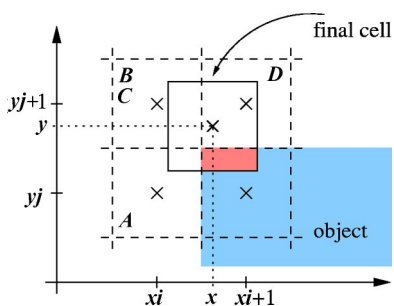


FIG. 4. Re-mapping of a final cell to mesh cells at a corner, when the moving cell overlaps a corner cell. The heavily shaded area marks the part of the final cell overlapping the obstacle. The velocities in cells A, B, and D are unchanged. Mesh cells B and C have the same index in configuration space, but their velocities are in opposite directions. (This is consistent with the rule described above for sphere-like corners.)

surface, a mirror cell is launched at the beginning of a time step for each real cell which will reflect off the surface. Half of the particles are in the original cell, the other half are carried in the mirror cell. The mirror cell starts at the mirror position with respect to the plane through the center of the mesh cell on the boundary in which the cell rebounds. Its velocity is the mirror velocity of the original cell. The cell and its mirror cell rebound on the surface obeying the rules of specular reflection described above. Hence, the tangential force is fully absorbed by the surface. The use of mirror cells in this way ensures that, since specular reflection as implemented here does not alter a homogeneous, isotropic gas, then neither does diffuse reflection. The ratio of the numbers of the particles in the initial cell and in its mirror cell can be adjusted, so that a different fraction of diffuse reflection can be achieved.

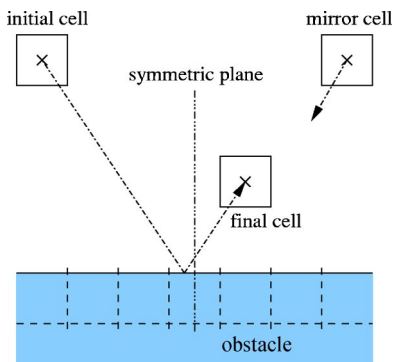


FIG. 5. Diffuse reflection. If a moving cell hits an obstacle in a time step, particles will be split evenly between the original cell and a mirror cell, which is a mirror image with respect to a symmetry plane located at the center of the boundary cell where the original cell reflects. This location of the mirror cell coincides with a real cell of the mesh. In a homogeneous, isotropic gas there will be no overall effect caused by the splitting since the mirror cell and the initial cell would have equal numbers of particles. The original and its mirror cell will annihilate the total tangential momentum of the particles. In this way, the properties of specular reflection are preserved, so an initially uniform static gas remains uniform and static.

III. CONSERVATION LAWS

In this section we discuss the collision operator, which is designed to exactly conserve various quantities, when implemented on a discrete mesh.

A. Conservation laws for scattered particles

Scattered particles are re-mapped in such a way that repeated application of the collision operator will yield a drift-Maxwellian distribution. The re-mapped particles have the same average (or drift) velocity and the same total kinetic energy, that the scattered particles had before they collided with each other. The use of a drift-Maxwellian or a similar distribution is essential, since other approximate forms for the distribution do not yield the correct values for off-diagonal elements of the stress [16]. (At each time step, the distribution which is added back may not be a Maxwellian—see Sec. III B—but for simplicity in this section we will refer to this distribution as a drift Maxwellian.)

However, the discreteness of the mesh complicates matters. Even though we use the nominal values of the drift velocity $V_x \hat{e}_x + V_y \hat{e}_y$ and the temperature T in the Maxwellian expression for the distribution at each grid point in velocity space, the actual values when summed over the entire distribution of scattered particles are different from their corresponding nominal values. For example, the nominal value for the x component of the drift velocity in a Maxwellian is different from the numerical one

$$V_x = \frac{NV_x}{N} \neq V_{x,num} = \frac{\sum_i v_{xi} \exp\{-m(\mathbf{v}_i - \mathbf{V})^2/2kT\} \Delta_i}{\sum_i \exp\{-m(\mathbf{v}_i - \mathbf{V})^2/2kT\} \Delta_i},$$

where the index i runs over the grid points of the velocity space mesh, Δ_i is the differential volume in the velocity space for the Riemannian sum, k is the Boltzmann constant, and N is the nominal value for the density. Similarly, other physical quantities, namely the y component of the drift velocity V_y , the temperature T , and the particle density N , will have different nominal values and corresponding numerical values.

For the purpose of the numerical simulation of the five-dimensional system (two-dimensional in configuration space, three-dimensional in velocity space), we have to conserve the particle density N , the total x -momentum NV_x , the total y -momentum NV_y , and the total kinetic energy $N\langle v^2 \rangle$ numerically for the scattered particles. In addition, the Maxwellian form of the distribution will automatically give reasonable values of higher moments of the distribution. Since there are more than four grid points on the velocity space mesh, to conserve the above four quantities numerically is generally possible. Let the corresponding numerical values be $(N)_1$, $(NV_x)_1$, $(NV_y)_1$, and $(N\langle v^2 \rangle)_1$. Intuitively there are several possibilities to re-map scattered particles back to the velocity space mesh with the various quantities conserved numerically. We now discuss several such methods.

The first method we considered turned out to be insufficiently robust. We began by scaling our first numerical estimate by a factor r , by matching $r(N)_1$ and N , so the errors will be

$$(N)' = N - r(N)_1 = 0, \quad (6)$$

$$(NV_x)' = NV_x - r(NV_x)_1, \quad (7)$$

$$(NV_y)' = NV_y - r(NV_y)_1, \quad (8)$$

$$(N\langle v^2 \rangle)' = N\langle v^2 \rangle - r(N\langle v^2 \rangle)_1. \quad (9)$$

Conditions on r are derived in the appendices. The scheme was iterated until the error was small; however, the convergence was poor.

A more robust scheme begins by scaling the discrete drift-Maxwellian distribution, based on the nominal values, N , $\langle V_x \rangle$, $\langle V_y \rangle$, and $N\langle v^2 \rangle$, in order to match N , the nominal number of scattered particles. With a reasonable velocity mesh, the error compared to the nominal drift Maxwellian is usually within 0.1%. Then we adjust the distribution to conserve the total kinetic energy. If the total kinetic energy is less than the nominal value, we move the particles from the cells in the lowest energy level to the cells in the highest energy level keeping the direction $(\mu|_\ell, \phi|_m)$ unchanged. (We stress that the required adjustments are very small but they are, nevertheless, important since conservation must be enforced locally and to high accuracy.) If all the particles in the lowest energy level are moved to the highest level and the total kinetic energy is still less than the nominal value, we can move the particles of the cells in the next lowest level. This procedure can be continued until the numerical kinetic energy matches the nominal value (and in reverse, if the total kinetic energy is more than the nominal value).

Finally, one can rearrange the particles within the same energy level to conserve momentum. Based on the design of the velocity space, if n particles are moved from the cell at (v, μ, ϕ) to the cell at $(v, \mu, \pi - \phi)$, the numerical value of the x component of the momentum for the scattered particles will be changed by $-2(nv\sqrt{1-\mu^2})\cos\phi$ while keeping the y component unchanged. Similarly, if n particles are moved from the cell at (v, μ, ϕ) to the cell at $(v, \mu, -\phi)$, the numerical value of the y component of the momentum for the scattered particles will be changed by $-2(nv\sqrt{1-\mu^2})\sin\phi$ while keeping the x component unchanged. The adjustments for x and y directions are thus decoupled. To make the adjustments evenly distributed among cells in velocity space, momenta in positive and negative directions are obtained first,

$$p_{x+} = \sum_{i \in x+} n_i (v\sqrt{1-\mu^2} \cos \phi)_i,$$

$$p_{x-} = \sum_{i \in x-} n_i (v\sqrt{1-\mu^2} \cos \phi)_i,$$

where $i \in x+$ is the index running over the cells with a positive x component of velocity, and $i \in x-$ with the negative. If $NV_x > (NV_x)_1$, we find the ratio

$$r = \frac{1}{2} \left(\frac{(NV_x)_1 - NV_x}{p_{x-}} \right).$$

This fraction of the scattered particles in the cell (v, μ, ϕ) , where $v\sqrt{1-\mu^2} \cos \phi$ is negative, is moved to the cell

$(v, \mu, \pi - \phi)$. If $NV_x < (NV_x)_1$, we find the ratio

$$r = \frac{1}{2} \left(\frac{(NV_x)_1 - NV_x}{p_{x+}} \right).$$

This fraction of the scattered particles in the cell (v, μ, ϕ) , where $v\sqrt{1-\mu^2} \cos \phi$ is positive, is moved to the cell $(v, \mu, \pi - \phi)$. A similar procedure can be applied to the adjustment of the y component of velocity. The adjustments in x and y are performed in alternate order as time advances, so there is no preference for either direction. In this way, the total particle number, the drift velocity, and the total kinetic energy of the scattered particles can be conserved very accurately in a drift-Maxwellian distribution. Experience shows this second scheme is more robust.

Another possibility is to construct a Maxwellian for each of a discrete set of nominal values of N , V_x , V_y , and T , and to store these in a table. Then the needed distribution can be constructed from a linear combination of the Maxwellians stored in the table. This will be examined in future work.

B. Collision operator

For the *BGK* collision operator in the *Krook* model [17]

$$\left(\frac{\partial f}{\partial t} \right)_c = -\nu(f - f_{\max})$$

the collision frequency ν is a constant obtained by averaging over the Maxwellian distribution of the background particles. If the collision frequency ν is not a constant, but a function of the incident particle velocity $\nu = N\sigma v$, where N is the background particle number density, σ is the collision cross section, and v is the particle velocity, then the scattered particles will be re-mapped back to the velocity mesh, with the following distribution:

$$\nu \Delta t f_{\max} = \Delta t N \sigma v \left(\frac{m}{2\pi kT} \right)^{3/2} \exp \left\{ -\frac{m(\mathbf{v} - \mathbf{V})^2}{2kT} \right\},$$

since this is the distribution of scattered particles which allows f to relax towards f_{\max} , as is implied by the Krook model. This nominal distribution for scattered particles is adjusted to conserve the particle number, momenta, and kinetic energy, as we described above.

IV. SIMULATION RESULTS AND DISCUSSION

The proper dimensionless number to specify the numerical experiments is the Knudsen number K_n . Since the transition regime is investigated in this paper, some dimensionless numbers considered in fluid dynamics become important when we approach the fluid dynamic regime. Following the canonical procedure in fluid dynamics with the characteristic length L and time τ , the BE with the Krook model can be cast into a *non-dimensionalized* form

$$\frac{\partial f}{\partial t^*} + \mathbf{v}^* \cdot \frac{\partial f}{\partial \mathbf{r}^*} + \mathbf{a}^* \cdot \frac{\partial f}{\partial \mathbf{v}^*} = K_n^{-1} v^* [f - f_{\max}(V, T)],$$

where $t^* = t/\tau$, $\mathbf{r}^* = \mathbf{r}/L$, $\mathbf{v}^* = \mathbf{v}\tau/L$, and $\mathbf{a}^* = \mathbf{a}\tau/L$. For a large K_n , the right hand side can be neglected, and the dy-

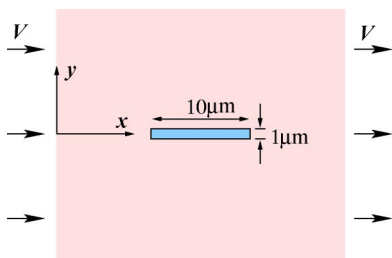


FIG. 6. Microflow system. A uniform argon gas with velocity V parallel to the plate at the center surrounds the simulation domain. The far-field flow velocity V is set to 40 m/s.

namics of the distribution are dominated by the *Vlasov equation*, which corresponds to the free molecular flow regime. On the other hand, if K_n is small, the distribution is expected to resemble a drift Maxwellian, in the fluid dynamics regime. Besides λ (or $1/N\sigma$, since $\tau=1/N\langle\sigma v\rangle$) and L , the flow speed V , the collision cross section σ , and the gas temperature T , also play roles in experiments. Using the *Buckingham π method* [18], it can be shown that the Euler number, the Reynolds number, and the Mach number are important system characteristics. The effects of these dimensionless parameters have been studied extensively in the literature on fluid dynamics.

A. System description

As shown in Fig. 6, argon gas is flowing in the x direction at room temperature (T is set to 0.025 eV, which is about 289 K). A thin plate with aspect ratio 10 is located in the middle of the simulation domain and parallel to the x axis.

The system dimension parallel to the far-field flow is chosen to be the characteristic length, $L=10 \mu\text{m}$. The argon atomic weight is about 40, so we set the collision cross section σ to be of the order of $10r_0^2$, where r_0 is the Bohr radius. To make the mean free path the same as L for the $K_n=1$ case, the number density is set about $4 \times 10^{24} \text{ m}^{-3}$. If we use the ideal gas equation for the argon gas, then the sound speed $\sqrt{\gamma kT/m}$ is of the order of 300 (m/s), where γ is the specific heat ratio 5/3, and the characteristic time τ is about 3×10^{-8} s. The argon viscosity μ is about $2.4 \times 10^{-4} \text{ N s/m}^2$, so the Reynolds number $\text{Re}=\rho VL/\mu$ is about 1100 for a flow velocity $V=40 \text{ m/s}$, where ρ is the argon mass density. The Mach number M is about 0.12. To resolve the collision process, the spatial cell size is set to less than 1/3 of the mean-free path, whose minimum is at $K_n=0.05$. The collision frequency depends on the velocity, since we assume hard-sphere collisions. The maximal collision frequency will occur for particles with maximal velocity on the mesh. The time step of the simulation is set to be less than 0.2 of the minimal collision time. The velocity resolution $\Delta v/v$ is set to 0.1 [9].

For this external flow problem, in addition to the diffuse reflection boundary condition (nonslip condition) on the obstacle, a buffer zone surrounds the simulation domain, so the distribution of particles which enter the simulation domain is fixed. The width of the buffer zone L_B is determined by the range of the velocity space mesh, such that cells with maxi-

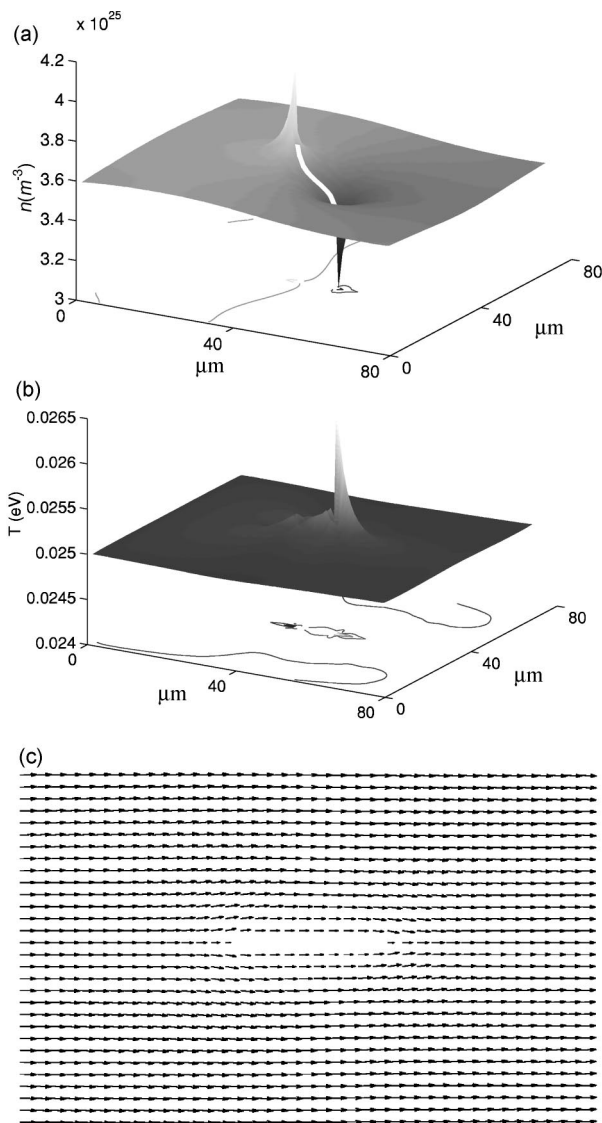


FIG. 7. Argon gas flow at $V=40 \text{ m/s}$, $K_n=1$, $T=0.25 \text{ eV}$: (a) Density profile. (b) Temperature Profile—the temperature fluctuates by about 2%. The friction around the obstacle generates the heat, which is carried to the downstream end of the plate by the flow. (c) Flow pattern—at low Reynolds number, there is no turbulence.

mal velocity from the domain are not able to cross the buffer zone in one time step

$$L_B \geq v_{\text{max}} \Delta t.$$

Cells in the buffer zone are described using a “0-dimensional” model, in that particles which leave the buffer zone and enter the main zone or which leave it on the outside are also reinjected into the buffer zone. The buffer zone is thus subject to periodic boundary conditions, while the buffer zone also injects particles into the main zone. In other words, the distribution in the buffer zone will be the same before and after ballistic motion; only the collision operator will change the buffer zone distribution. We assume hard-sphere collisions between neutral argon particles. The density, the flow velocity, and the temperature in the buffer zone

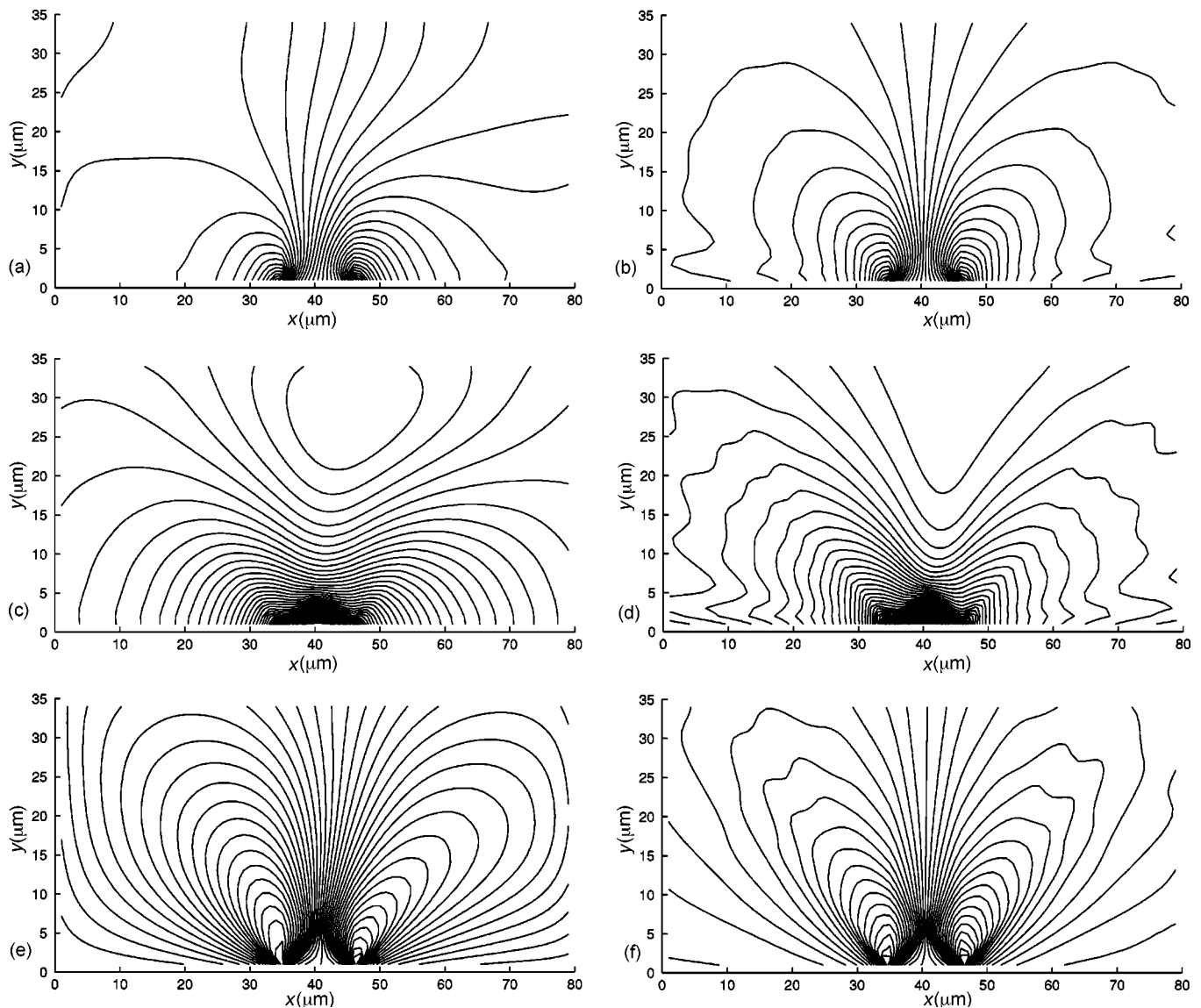


FIG. 8. Contours for density and velocity profiles: Far-field flow velocity is $40\hat{e}_x+0\hat{e}_y$ (m/s) (a) The contours represent intervals of 6.4×10^{22} (m^{-3}), from the maximum of 3.57×10^{25} (m^{-3}) on the boundary. (b) The contours represent intervals of 1.1×10^{22} (m^{-3}), from the maximum of 3.57×10^{24} (m^{-3}) on the boundary. (c) The contours represent intervals of 0.56 (m/s), (d) The contours represent intervals of 0.40 (m/s), (e) The contours represent intervals of 0.28 (m/s), from the maximum of 5.38 (m/s) on the left end of the plate to the minimum of -5.62 (m/s) on the right end of the plate. (f) The contours represent intervals of 0.28 (m/s), from the maximum of 5.84 (m/s) on the left end of the plate to the minimum of -6.57 (m/s) on the right end of the plate.

are kept constant throughout the run to set up the far-field boundary condition.

Since computer resources are limited, we also tested the effects on the simulation results of the resolution, i.e., the size of the numerical mesh. In most simulation runs, the simulation domain is a uniformly spaced mesh with 100 grid points in the x direction, $N_x=100$, and 100 grid points in the y direction, $N_y=100$. For each spatial cell point, there are 32 grid points in v , $N_v=32$, 8 in μ , $N_\mu=8$, and 32 in ϕ , $N_\phi=32$. (Smaller numbers gave results which were not converged with respect to the mesh size.) Each cell has two variables (one for the current time step, the other for next time step), and each double precision variable takes 8 bytes. Hence, for this size of mesh there are about 400 megabytes of computer memory used in each simulation run.

B. Density and velocity profiles

As shown in Fig. 7(a), where the flow velocity is 40 m/s, and $K_n=1$, density builds up at the upstream end of the plate, and is depleted at the downstream end. Around the plate there is a roughly 2% fluctuation in temperature. All these flows have low Reynolds numbers, as shown in Fig. 7(c); the flow pattern is laminar, there is no turbulence. Since the simulation results are symmetric with respect to the x axis, only half of the domain is shown on the figures in the following discussion.

The contour plots of the density, the x component of the flow velocity, and y component of the flow velocity, for $K_n=1$ and $K_n=10$, are shown in Fig. 8. The far-field flow velocity is $40\hat{e}_x+0\hat{e}_y$ (m/s) for both cases. Both density pro-

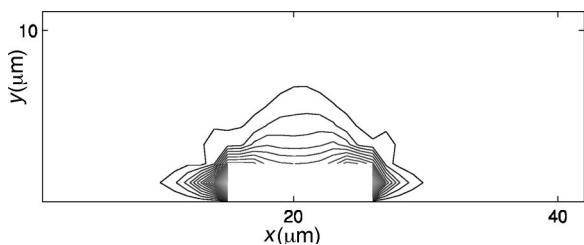


FIG. 9. Contour plot of the magnitude of the strain rate.

files have a peak at the upstream (left) end of the plate. Since the plate surface is a discontinuity, the peak of the density should be infinitesimally close to the plate, but not on the plate surface. The density drops gradually to a minimal value at the downstream (right) end of the plate. Due to the nonslip condition, the x component of the flow velocity on the surface of the plate is actually zero. Since the Mach number is less than 0.12 in this study, the argon gas can be considered as incompressible in the fluid dynamic regime. Based on the conservation of mass, the flow velocity above the plate can be greater than the far-field flow velocity. This phenomenon is also observed in the free-molecular flow regime $K_n \geq 1$, as shown in Figs. 8(c) and 8(d). In the upper half region the y component of the flow velocity has a positive maximum near the upstream end of the plate, and a negative minimum near the downstream end. The results qualitatively agree well with other simulations [16].

The profiles are more symmetric in the x direction as K_n becomes larger, since the characteristic length of the flow is the mean-free-path λ . As λ approaches ∞ , the plate degenerates to a *doublet* point, if we keep the aspect ratio of the plate constant.

The region where the plate starts to affect the flow can be revealed by the contour plot of the following function which describes the magnitude of the strain rate

$$\sqrt{\left| \frac{\partial V_x}{\partial y} \right|^2 + \left| \frac{\partial V_y}{\partial x} \right|^2}.$$

A contour plot of the strain rate for $K_n=1$ is shown in Fig. 9. For a Newtonian fluid, the stress is linearly proportional to the strain rate.

C. Drag coefficient

The CS enforces the conservation of momentum precisely. This feature is very important in calculating the drag and the lift of an object against a flow. The drag force parallel to the far-field flow is usually studied in terms of the drag coefficient. The definition of the drag coefficient in our calculation is

$$C_d = \frac{F_x/A}{\rho V^2/2},$$

where F_x/A is the averaged shear stress parallel to the free flow, ρ is the gas mass density, and V is the free flow velocity. Normal force due to the pressure on the plate is not included in the calculation. As shown in Table I, the change of the drag coefficient mostly takes place for $K_n \approx 0.2$.

TABLE I. The drag coefficient C_d . The flow velocity V of the argon gas is 40 m/s.

K_n	CS C_d	IP C_d	DSMC C_d
0.05	1.50	1.45	1.52
0.2	3.36	3.00	3.04
0.8	3.87	4.62	4.25
1.2	4.12	4.81	4.76
10	4.88		

Comparison of the drag coefficient with data from particle simulations [16] is shown in Fig. 10. The results from the information preserving (IP) and direct simulation Monte Carlo (DSMC) methods are based on a nonuniform mesh. The flow velocity is the same for all methods. The methods appear to give reasonable agreement as to the drag coefficient, which is a rather sensitive test and probably shows differences more than most other comparisons. The major discrepancy we observe is that the particle simulations go to the free molecular flow limit soon after $K_n=1$, whereas the CS simulation is a little slower to reach the asymptote. All the methods show rather different flow patterns at $K_n=1$ as compared to $K_n=\infty$, so we might expect some difference between C_d in the two cases. The particle methods appear to differ from each other by as much as 20%, suggesting that this is the error associated with the calculations. The CS results also agree with the particle methods, to within this error.

V. CONCLUSIONS

The CS is an alternative to particle methods for solving the Boltzmann equation, which does not suffer from statistical noise, and which is suitable for the transition regime, $K_n=0.05$ to $K_n=10$. With a suitable design of the velocity mesh, flow around complicated geometric objects can be studied using the CS. Numerical diffusion in velocity space is largely avoided; numerical diffusion in physical space is minimized by the long time steps which are permissible in

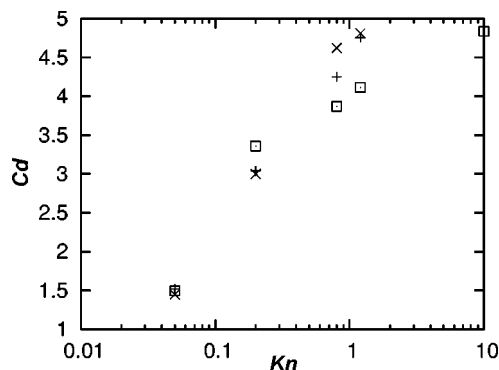


FIG. 10. Drag coefficient C_d vs K_n . Uniform meshes are used for the CS (\square). IP (\times) and DSMC ($+$) data are based on a nonuniform mesh. The far-field flow velocity is 40 (m/s).

the CS. Conservation of particles, conservation of momentum, and conservation of energy, which are crucial both in fluid dynamics and rarefied gas dynamics, are implemented exactly, numerically in the CS. We presented schemes to handle reflections and collisions very precisely. Comparison to particle simulations was briefly presented. It was shown that the convective scheme gives results in agreement with earlier work [16] with regard to the drag coefficient, which is a somewhat sensitive test of the collision operator.

APPENDIX A: INTRODUCTION TO THE CONVECTIVE SCHEME (CS)

Based on using the propagator method, the CS solves the Boltzmann equation for the (one-particle) distribution function. In contrast to tracing super particles in particle methods [19,20], the distribution function is treated as a phase-space fluid by the CS. For each particle species the formal solution of the Boltzmann equation for short time steps can be written as

$$f(\mathbf{x}, \mathbf{v}, t) = \int \int \mathcal{P}(\mathbf{x}, \mathbf{v}, t; \mathbf{x}', \mathbf{v}', t') f(\mathbf{x}', \mathbf{v}', t') d\mathbf{x}' d\mathbf{v}', \quad t > t' \quad (\text{A1})$$

where the kernel of the integral, $\mathcal{P}(\mathbf{x}, \mathbf{v}, t; \mathbf{x}', \mathbf{v}', t')$, is the propagator for a particle at the phase-space position $(\mathbf{x}', \mathbf{v}')$ at time t' moving to (\mathbf{x}, \mathbf{v}) at a later time t . Certain properties and conservation laws related to this propagator in the CS were noted by Adams and Hitchon [21]. Instead of finding the explicit form of the propagator in a 14-dimensional space, the CS propagator is broken into two parts—one for the ballistic motion and one for collisions. In the ballistic motion collisions are neglected, and the Boltzmann equation is reduced to the *Vlasov equation*

$$\frac{df}{dt} = \frac{\partial f}{\partial t} + \mathbf{v} \cdot \frac{\partial f}{\partial \mathbf{x}} + \mathbf{a} \cdot \frac{\partial f}{\partial \mathbf{v}} = 0. \quad (\text{A2})$$

Deceptively in this linear form, the Vlasov equation is actually an integrodifferential equation, since the electromagnetic forces in the term \mathbf{a} are derived from Maxwell's equations as integrals of the charge and current densities, which depend on the distribution functions of charged particles. In the CS, the Vlasov equation is numerically integrated along the *characteristic curves*, which are determined by the equations of motion: $d\mathbf{x}/dt = \mathbf{v}$ and $d\mathbf{v}/dt = \mathbf{a}$. After this ballistic motion step is complete for all particle species, f is adjusted according to the collision processes described by the collision operators $C(f)$ as well as chemical reactions. Usually the Krook collision operator or the Coulomb collision operator [17] and some other collision processes, like ionization and excitation, are incorporated into the collision operators. Recombination in weakly ionized plasmas can be incorporated likewise.

Since particles in a cell are uniformly distributed over the space with the same velocity, rules similar to Eqs. (2)–(5) are used to map unscattered particles in the final cell to the mesh cells. Mesh cells may have different potential energy levels, so care must be taken to conserve the relative physical quan-

ties, such as the particle number and the total energy. Scattered particles are put back to the mesh cells with the same spatial index but different velocity index according to the collision operator, which can account for elastic or inelastic collisions. The particle number for scattered particles can also be changed if source or sink terms are present in the collision operator.

APPENDIX B: ALTERNATIVE IMPLEMENTATION OF CONSERVATION LAWS

Using the scaling of Eq. (9), $(N\langle v^2 \rangle)'$ could be negative, which is undesirable in this scheme, where we will add additional particles back to correct for errors—negative density or energy would be unphysical. Therefore, we set an inequality for r

$$r \leq \min \left\{ \frac{N}{(N)_1}, \frac{N\langle v^2 \rangle}{(N\langle v^2 \rangle)_1} \right\}. \quad (\text{B1})$$

The temperature for the particles is $T' = m[(N\langle v^2 \rangle)'(N)' - (NV_x)'^2 - (NV_y)'^2] / (3KN'^2)$. Since a negative temperature [22] is not possible for this system, we obtain another inequality for r from $T' \geq 0$. Furthermore, although the z component of the flow velocity is zero, if there is no grid points on the velocity space mesh with $v_z = 0$, then $\langle v_z^2 \rangle > 0$. Let the maximal projection of the velocity grid points on the xy plane be $v_{\max} p$, where $p = \sqrt{1 - \mu_{\min}^2}$, μ_{\min} is the minimal value of $\mu = \cos \theta$ on the grid points, and θ is the angle of the velocity with respect to the z axis. The following inequality will guarantee the error can be described by a group of particles with a drift-Maxwellian distribution:

$$\frac{(N\langle v^2 \rangle)'}{(N)'} p^2 \geq \left(\frac{(NV_x)'}{(N)'} \right)^2 + \left(\frac{(NV_y)'}{(N)'} \right)^2.$$

The original nominal values (or any numerical drift-Maxwellian distribution) also satisfy the above inequality. After some algebraic steps, the above inequality for r can be written as $Ar^2 + Br + C \geq 0$, where $A = p^2(N)_1(N\langle v^2 \rangle)_1 - (NV_x)_1^2 - (NV_y)_1^2$, $B = 2\{NV_x(NV_x)_1 + NV_y(NV_y)_1\} - p^2\{N\langle v^2 \rangle(N)_1 + N\langle v^2 \rangle_1\}$, and $C = p^2 NN\langle v^2 \rangle - (NV_x)^2 - (NV_y)^2$. As mentioned above, we know that $A \geq 0$ and $B \geq 0$, and the equal sign holds only when all the particles have the same velocity.

Another possibility is to treat the error as a group of particles with the same velocity, which should fall within the velocity space mesh. Then we have two more inequalities

$$v_{\min}^2 \leq \frac{(N\langle v^2 \rangle)'}{(N)'} \leq v_{\max}^2,$$

where v_{\max} and v_{\min} are the maximal and minimal velocities in the velocity space mesh, respectively. The original nominal values (or any numerical drift-Maxwellian distribution) also satisfy the above two inequalities. After some algebraic steps, they can be written as

$$r \leq \min \left\{ \frac{N\langle v^2 \rangle - Nv_{\min}^2}{(N\langle v^2 \rangle)_1 - (N)_1 v_{\min}^2}, \frac{Nv_{\max}^2 - N\langle v^2 \rangle}{(N)_1 v_{\max}^2 - (N\langle v^2 \rangle)_1} \right\} \quad (\text{B2})$$

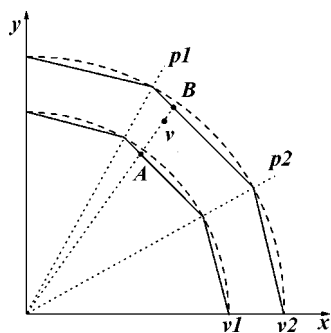


FIG. 11. Conservation of momentum. The range of the perpendicular velocity of particles with a fixed energy level is a polygon. If the average velocity V of the scattered particles is in the area between 2 polygons based on v_1 and v_2 , it can be expressed as a linear combination of velocities at A and B which are linear combinations of grid points at ϕ_1 and ϕ_2 . If the average velocity is within the inner polygon, it is possible to conserve momentum and energy at the same time for the scattered particles when remapping back to the mesh cell.

We can use the error values as a new set of nominal values for a group of drift-Maxwellian particles, and let the second set of numerical estimates be $(N)_2$, $(NV_x)_2$, $(NV_y)_2$, and $(N\langle v^2 \rangle)_2$. By choosing an r that satisfies inequalities (B1)–(B2), we will get a new set of error values: $(N)''$, $(NV_x)''$, $(NV_y)''$, and $(N\langle v^2 \rangle)''$. This procedure can be continued, if we make the error in the particle density less than e^{-1} of the nominal value, i.e., choosing r 's such that $Ne^{-1} \geq N'$, $N'e^{-1} \geq N''$, and so on. Generally we can get four estimates

and the final error values will be \tilde{N} , $\overline{NV_x}$, $\overline{NV_y}$, and $N\langle \tilde{v}^2 \rangle$. Sometimes, we can find a linear combination of these four estimates that will match all the original nominal values: $N = \sum_{i=1}^4 C_i(N)_i$, $NV_x = \sum_{i=1}^4 C_i(NV_x)_i$, $NV_y = \sum_{i=1}^4 C_i(NV_y)_i$, and $N\langle v^2 \rangle = \sum_{i=1}^4 C_i(N\langle v^2 \rangle)_i$. Unknown coefficients C_i are required to be non-negative. Otherwise, we have to remap the final error back to the velocity space. Note that $\tilde{N} \leq e^{-4}N$ usually, so it is a small perturbation of the linear combination of the drift Maxwellians.

To map back the group of particles with the nominal values \tilde{N} , $\overline{NV_x}$, $\overline{NV_y}$, and $N\langle \tilde{v}^2 \rangle$, we assume they have the same velocity. We define $\tilde{V}_x = \overline{NV_x} / \tilde{N}$, $\tilde{V}_y = \overline{NV_y} / \tilde{N}$, $\tilde{V} = \sqrt{N\langle \tilde{v}^2 \rangle} / \tilde{N}$, and find the two grid points v_1 and v_2 between which \tilde{V} is located. There is a number $0 \leq r_e \leq 1$ such that $\tilde{V}^2 = r_e v_1^2 + (1 - r_e)v_2^2$. Similarly, as shown in Fig. 11, the velocity $V = \tilde{V}_x \hat{e}_x + \tilde{V}_y \hat{e}_y$ is a linear combination of points A and B which can be built up by using different μ grid points with azimuthal grid points ϕ_1 and ϕ_2 on the velocity space mesh. Since V should be located in the polygon area, the p value in the inequalities $Ar^2 + Br + C \geq 0$ can incorporate the factor accounting for the discreteness of the azimuthal angle: $p = \sqrt{1 - \mu_{\min} \cos(\Delta\phi/2)}$, where $\Delta\phi$ is the space between two ϕ grid points. More sophisticated schemes for p can be implemented to alleviate the constraint. Once the projections on the ϕ_1 and ϕ_2 directions are found, we can adjust the numbers of particles among μ cells to match the projection in each direction. In principle the momentum and the kinetic energy cannot always be conserved at the same time. In that case, we choose to conserve the momentum.

[1] S. Vargo and E. Muntz, *22nd International Symposium on Rarefied Gas Dynamics, Sydney, Australia, July 2000*, edited by Timothy J. Bartel and Michael A. Gallis (AIP, Melville, NY, 2001), p. 502.

[2] H. Tuan, H. Janssen, C. Cramers, P. Mussche, J. Lips, N. Wilson, and A. Handley, *J. Chromatogr.*, A **791**, 187 (1997).

[3] A. Segal, T. Górecki, P. Mussche, J. Lips, and J. Pawliszyn, *J. Chromatogr.*, A **873**, 13 (2000).

[4] F. Chen, *Introduction to Plasma Physics and Controlled Fusion*, 2nd ed. (Plenum, New York, 1984), Vol. 1.

[5] Q. Sun, I. Boyd, and G. Candler, *J. Thermophys. Heat Transfer* **16**, 171 (2002).

[6] Q. Sun and I. Boyd, *J. Comput. Phys.* **179**, 400 (2002).

[7] W. Hitchon, D. Koch, and J. Adams, *J. Comput. Phys.* **83**, 79 (1989).

[8] D. Koch and W. Hitchon, *Phys. Fluids B* **1**, 2239 (1989).

[9] J. Feng and W. Hitchon, *Phys. Rev. E* **61**, 3160 (2000).

[10] V. Aristov, *Direct Methods for Solving the Boltzmann Equation and Study of Nonequilibrium Flows* (Kluwer, Dordrecht, 2001).

[11] Z. Li and H. Zhang, *J. Comput. Phys.* **193**, 708 (2004).

[12] A. Christlieb, W. Hitchon, and E. Keiter, *IEEE Trans. Plasma Sci.* **28**, 2214 (2000).

[13] A. Christlieb and W. Hitchon, *Phys. Rev. E* **65**, 056708 (2002).

[14] W. N. G. Hitchon, G. J. Parker, and J. E. Lawler, *IEEE Trans. Plasma Sci.* **22**, 267 (1994).

[15] G. Parker, W. Hitchon, and J. Lawler, *Phys. Rev. E* **50**, 3210 (1994).

[16] A. Christlieb, W. Hitchon, Q. Sun, and I. Boyd, *23rd International Symposium on Rarefied Gas Dynamics, Whistler, British Columbia, Canada, July 2002*, edited by Andrew D. Ketsdever and E. P. Muntz (AIP, Melville, NY, 2003).

[17] K. Miyamoto, *Plasma Physics for Nuclear Fusion* (MIT, Cambridge, MA, 1989), revised ed.

[18] R. Pao, *Fluid Dynamics* (Merrill, Columbus, OH, 1967).

[19] R. Hockney and J. Eastwood, *Computer Simulation Using Particles* (IOP, Bristol, England, 1988).

[20] C. Birdsall and A. Langdon, *Plasma Physics via Computer Simulation* (McGraw-Hill, New York, 1985).

[21] J. Adams and W. Hitchon, *J. Comput. Phys.* **76**, 159 (1988).

[22] F. Reif, *Fundamentals of Statistical and Thermal Physics* (McGraw-Hill, New York, 1965).